ELSEVIER

International Journal of Mass Spectrometry 220 (2002) 159–170

International Journal of Mass Spectrometry

www.elsevier.com/locate/ijms

Cage effects and rotational hindrance in the surface scattering of large $(N_2)_n$ clusters

Nihed Chaâbane[a], Gregor Jundt[a], Holger Vach[a,*], Denise M. Koch[b], Gilles H. Peslherbe[b]

[a] *Laboratoire de Physique des Interfaces et des Couches Minces (UMR7647 CNRS) Ecole Polytechnique, 91128 Palaiseau Cedex, France*
[b] *Department of Chemistry and Biochemistry, Centre for Research in Molecular Modeling (CERMM), Concordia University, Montréal, Québec, Canada H3G 1M8*

Received 5 October 2001; accepted 2 April 2002

Abstract

We present results from classical trajectory calculations of collisions of $(N_2)_n$ ($64 \leq n \leq 512$) clusters with a graphite surface in order to deepen our understanding of energy transfer processes and cluster fragmentation dynamics. Translational and rotational distributions for the monomer products of evaporation are determined for incidence angles between 30 and 70°, at an incident velocity of 750 ± 50 m s^{-1} and for two surface temperatures. Our molecular dynamics simulations, which employ a simple trapping/desorption model for describing the interactions between molecules and the surface, allow us to reproduce experimental results not only qualitatively, but also quantitatively. A detailed analysis of the scattering event shows that the monomer translational energy distributions can be well described by a single Boltzmann distribution, while the rotational distributions of scattered molecules are best represented by a sum of two distinct Boltzmann distributions. The two resulting rotational temperatures can be attributed to a significant cage effect occurring during the cluster–surface impact. As a result, monomers originating from the outskirts of the clusters evaporate rotationally hot, while monomers from the very interior of the cluster—which are subject to cage effects—tend to be rotationally colder. Absolute values of the rotational temperatures indicate that the hot monomers experience significant rotational hindrance when evaporating from their parent cluster. (Int J Mass Spectrom 220 (2002) 159–170)

Keywords: Nitrogen clusters; Molecular dynamics simulations; Cluster–surface interaction; Energy exchanges; Rotational hindrance; Translational temperature; Cluster size dependence

1. Introduction

Recently, theoretical studies [1] have predicted that reactions with large activation barriers could occur under the extreme conditions that are produced within clusters upon impact with a solid surface. In order to gain some insight into the dynamics of this so-called "chemistry with a hammer" [2], elementary energy transfer processes to internal degrees of freedom should be well understood. In the past, experimental [3–11] and theoretical [12–17] studies have concentrated mainly on the scattering of atomic van der Waals clusters, where only energy transfer to translational degrees of freedom is possible. Only recently, the rotational and translational distributions of the products of nitrogen cluster scattering have been measured using (REMPI) and quadrupole mass spectrometry [18]. Motivated by the difficulty to explain some of the experimental results, we engaged into molecular dynamics simulations, of which a preliminary

* Corresponding author. E-mail: vach@leonardo.polytechnique.fr

1387-3806/02/$ – see front matter
PII S1387-3806(02)00690-5

account has been given elsewhere [19]. While the qualitative trends observed experimentally were well reproduced in our previous simulations, the agreement between simulations and experiment was not quantitative. In this article, we present simulation results with a simple phenomenological trapping/desorption model that allows us to reproduce all previous experimental data quantitatively, and to understand the details of energy flow between all molecular degrees of freedom and the surface. For instance, the hindered-rotation problem is an important topic in the study of both the rotation of molecules bound inside a crystal [20] and the overall rotation of molecules adsorbed on solid surfaces [21]. The lack of clear understanding of energy transfer processes becomes yet more important when the interacting entities become as complex as large clusters and solid state surfaces.

2. Computational method

Most of the computational details have been described previously [19], so we limit our discussion here to the most important features of the simulation procedure and the new features of the present study. The trajectories were propagated in time by integrating Newton's equations of motion [22] with a fifth-order Gear algorithm [23] and a fixed step size of 0.2 fs. The intramolecular N–N interactions are modeled by Morse potentials [24] and the intermolecular N_2–N_2 van der Waals interactions by four-center N–N standard Lennard–Jones potentials [25].

All simulations reported here involve collisions between large neutral nitrogen clusters and a hard surface at an incidence angle θ_i (measured from the surface normal) between 30 and 70°, with nitrogen $(N_2)_n$ clusters thermalized at 32 K [26] and ranging in size from 64 to 512 molecules per cluster, and at an incoming cluster velocity of 750 m s^{-1} [18]. To account for the energy transfer between the surface and the scattering cluster, we employed the lost memory model [27] for quasi-trapping [28]. In this model, we calculate the probability β for an individual, incoming particle to become trapped as

$$\beta = \exp\left(-\frac{E_n}{E_s}\right)$$

where E_n is the normal kinetic energy $mv_z^2/2$, with v_z being the normal velocity component if the surface is in the (x, y) plane as shown in Fig. 1. E_s in the above equation is the surface–molecule binding energy, which is taken as the experimentally determined value of 10.05 kJ mol^{-1} [29] in the present study. In our model, each monomer that becomes trapped on the surface transfers the kinetic energy that corresponds to its normal velocity component to the surface. Once trapped, the monomer remains on the surface during a residence time τ that is determined by the surface temperature T_s and the surface–molecule binding energy E_s as

$$\tau = \left(\frac{h}{k_B T_s}\right) \exp\left(\frac{E_s}{k_B T_s}\right)$$

where h is Planck's constant and k_B Boltzmann's constant [30].

At the end of their residence time τ, monomers receive an amount of energy from the surface that corresponds to its temperature and desorb in a random direction [27]. Those molecules that do not get trapped on the surface are assumed to suffer an elastic "reflection" from the hard surface, i.e., we simply reverse their normal velocity component upon surface impact [19,27]. In order to compare to experimental results, we calculate the parallel velocity conservation coefficient c_F that is determined by the ratio of the final and the initial tangential velocity components of the largest surviving cluster. Once an evaporated monomer is at a distance of 6.5 Å [16] from all other monomers, we determine their rotational, vibrational and translational energies. To average out possible vibrational–rotational coupling, E_{rot} is averaged over several vibrational periods of the monomers. Vibrational and rotational quantum numbers can then be obtained by semi-classical quantization [31]. As in the experimental study [18], the translational energies of the evaporated monomers are defined with respect

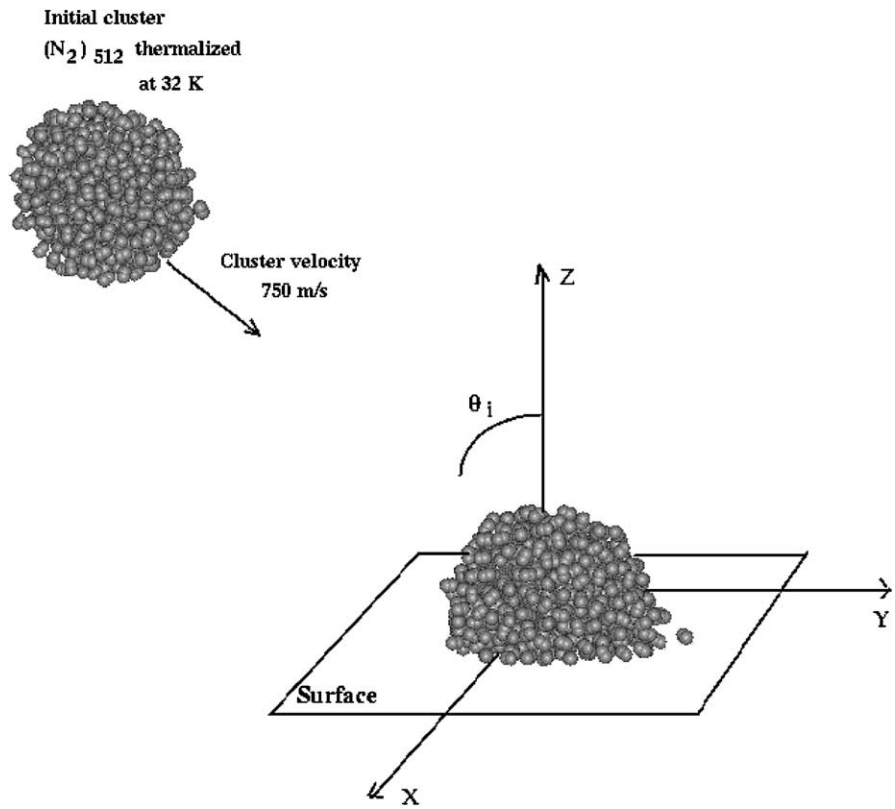

Fig. 1. Schematic diagram of the coordinate system employed in our simulations of cluster surface collision.

to the center of mass of the largest surviving cluster fragment.

3. Results and discussion

Fig. 2 depicts the dynamics of the scattering of a nitrogen cluster. As the cluster becomes compressed upon the surface, intermolecular and surface collisions result in the rapid heating of the cluster and a drastic increase in the cluster temperature. This heating causes evaporation of nitrogen monomers that have gained translational energy from cluster–surface impact. In the following, we will first determine the fraction c_F of the initial parallel velocity component of the incident cluster that is conserved by the biggest surviving cluster fragment. Then, we will analyze the translational and rotational distributions for the evaporated N_2 monomers.

3.1. Parallel velocity conservation factor c_F for the surviving cluster

Values of c_F are shown in Fig. 3 for two different surface temperatures and for several initial clusters sizes. Except for very small incidence angles, the coefficient c_F always remains at 1.00 ± 0.08, in excellent agreement with experiment; i.e., the outgoing fragments conserve about all of their incident parallel velocity component. The coefficient c_F increases rapidly for θ_i smaller than 40°, and reaches values up to 1.5 at an incidence angle of 30°. This gain of parallel velocity component suggests that not all of the incident normal kinetic energy is used for the

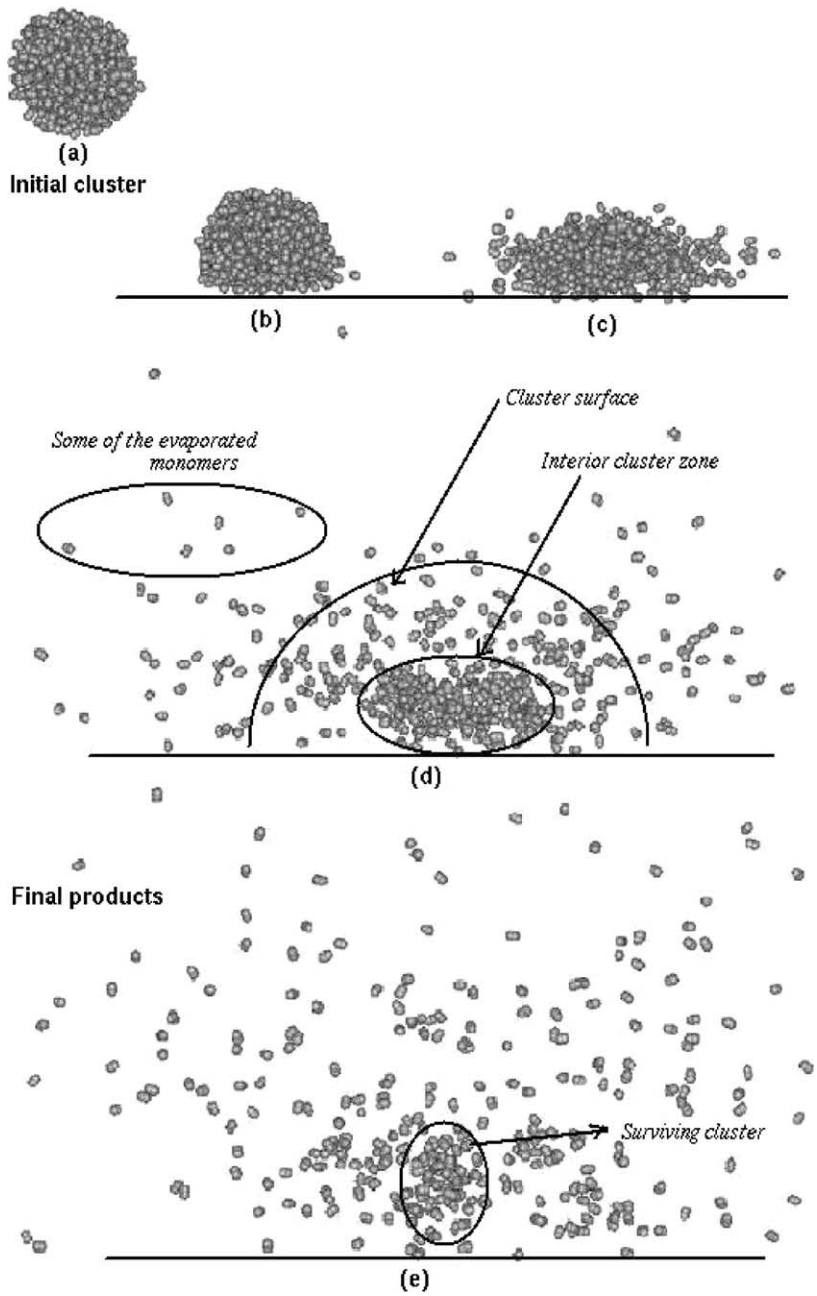

Fig. 2. Five typical snapshots of the surface scattering at different times for a 60° incidence angle: (a) the initial cluster of 512 molecules ($t = 0$ ps); (b) just at cluster–surface impact; (c) directly after the deposition of the $(N_2)_{512}$ cluster on the surface; (d) intermediate step where monomers evaporation takes place; (e) after 100 ps where the major part of the cluster has evaporated.

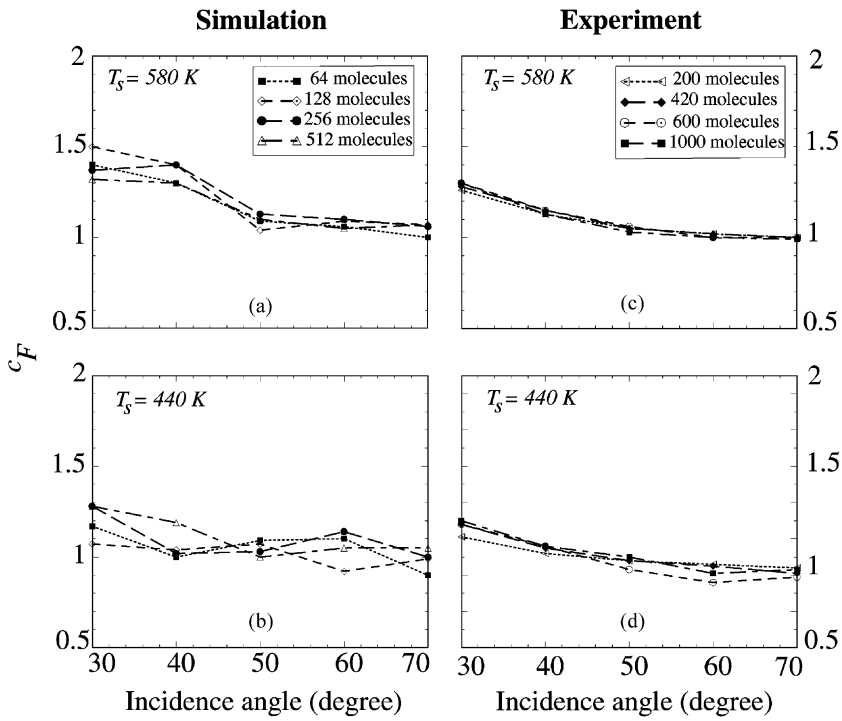

Fig. 3. Simulated and measured parallel velocity conservation coefficients as a function of incident angle, incident cluster size, and surface temperature.

thermalization and evaporation of N_2 molecules, but that part of it is transferred to the tangential velocity component, as previously discussed for argon clusters [32].

Fig. 3(a) and (b) display c_F profiles for surface temperature values of 580 and 440 K, respectively. When the surface temperature decreases, parent clusters gliding on the graphite surface are slowed down, as can be seen from a decrease in the c_F coefficient [33]. Both simulation and experimental data indicate that the observed c_F values do not vary with incident cluster size. This observation might at first appear surprising, since one might expect that larger clusters deform the surface more and should thus experience more friction, resulting in a smaller c_F value. The observed independence suggests that most monomers of the cluster do not interact directly with the surface, but rather with other nitrogen atoms between the cluster and the surface [32]. Therefore, we propose that a portion of the cluster monomers will become "trapped" between the surface and the incoming cluster, creating an isolating cushion (see Fig. 2(d)), as will be discussed below in the light of the dynamic zone structure (DZS) model [16].

3.2. Translational distributions of the evaporating monomers

As in experiments, the translational temperatures T_{trans} of the evaporated products were determined by fitting the simulated translational energy distributions by single Maxwell–Boltzmann distributions. These temperatures turned out to be thermalized at the instantaneous cluster temperature and to decrease with increasing incident angle θ_i. These qualitative findings are in good agreement with our previous experimental and simulation results [18,19]. The more realistic surface model employed in the present work leads

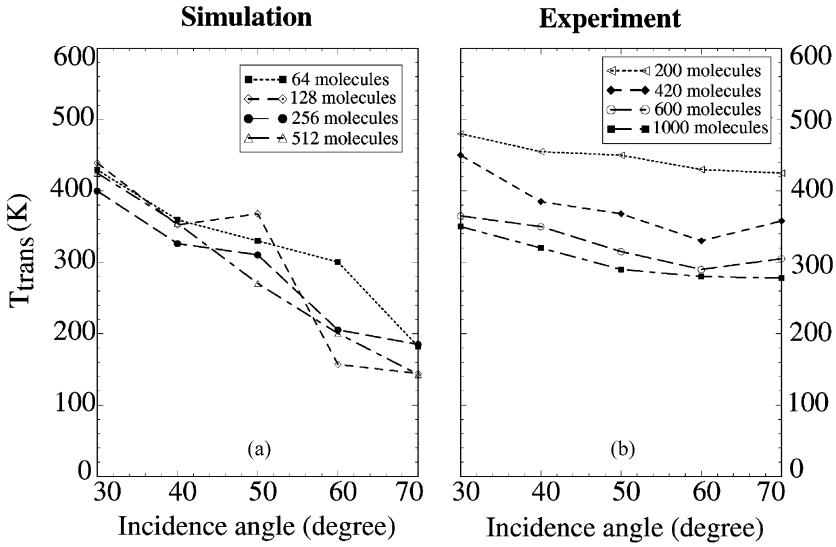

Fig. 4. Evolution of the translational temperature with incident angle and cluster size.

to an excellent quantitative agreement between simulated and measured values for all incidence angles smaller than 60°, as shown in Fig. 4. At this point, we would like to point out that our surface model does not contain any adjustable parameter. One could obviously obtain a yet better agreement for T_{trans}, even for the largest incidence angles, by using the surface–molecule binding energy as a fit parameter. In this work, however, we prefer to demonstrate that we can achieve a very good agreement between simulation and experiment, even when simply fixing E_s to its experimentally determined value of 10.05 kJ mol^{-1} [29]. The observed increase in the translational temperatures with decreasing θ_i, shown in Fig. 4, can be explained by the more violent cluster compression during surface impact which favors energy transfer from translational to internal degrees of freedom. It is well known that the degree of cluster heating scales with the normal component of the incident kinetic energy [16]. In Fig. 5(a), we display the instantaneous cluster temperature $T_{cluster}$ calculated from the kinetic energy of all cluster molecules in the moving cluster frame. For two different incidence angles, we show that $T_{cluster}$ increases until the evaporation process starts taking place. Thereafter, the cluster temperature

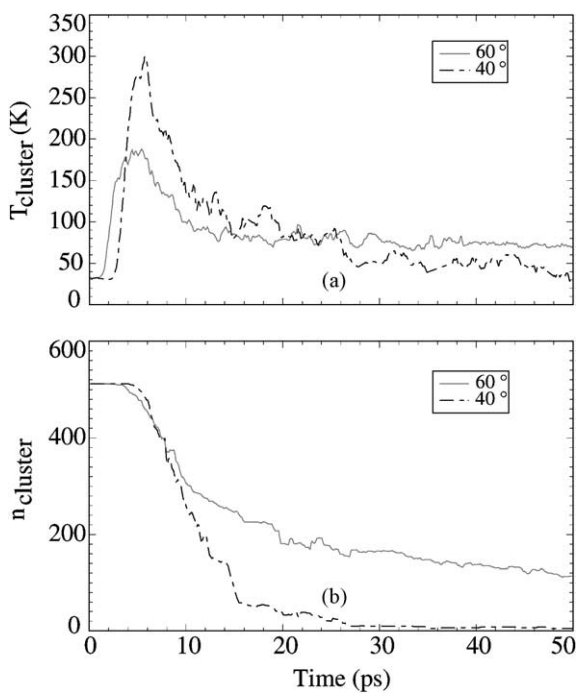

Fig. 5. (a) Instantaneous cluster temperature $T_{cluster}$ averaged over all cluster molecules and (b) number of molecules in the surviving cluster for 40 and 60° incidence angles, with an initial cluster size of 512 molecules and $T_s = 580$ K. Time "$t = 0$" corresponds to the beginning of our trajectory calculations.

decreases as a function of time. The maximum cluster temperature is obviously higher for an incidence angle of 40° than for 60°, because there is a larger amount of normal kinetic energy available to heat the cluster. A few picoseconds after the beginning of monomer evaporation, $T_{cluster}$ stabilizes at a constant value for both incidence angles. However, the stabilized cluster temperature is higher for a 60° incidence angle than for 40°, because many more evaporated monomers participated in the cluster cooling process in the latter case (see Fig. 5(b)).

3.3. Rotational distributions of the evaporating monomers

As stated above, the translational energy distribution of the evaporating molecules can well be described with a single Maxwell–Boltzmann distribution; i.e., with one single temperature T_{trans}. The rotational energy distributions, however, cannot be described by a single thermal distribution. Fig. 6(a) and (c) show the calculated translational and rotational energy distributions $P(E_{trans})$ and $P(E_{rot})$ resulting from the scattering process. Corresponding logarithmic plots in Fig. 6(b) and (d) show a linear dependence of $\log P(E_{trans})$ on the translational energy E_{trans}, while $\log P(E_{rot})$ vs. E_{rot} can only be satisfactorily represented by a sum of two rotational Boltzmann distributions which, indeed, confirms the experimental observation of two rotational temperatures.

In Fig. 7(a), we show the resulting rotational temperatures as a function of incidence angle for different cluster sizes. The cold component is essentially constant and equal to the experimental values of 75 ± 20 K, whereas the hot temperatures are around 375 K which is also in excellent agreement with previous experiment (see Fig. 7(b)), especially when considering the 16% experimental uncertainty.

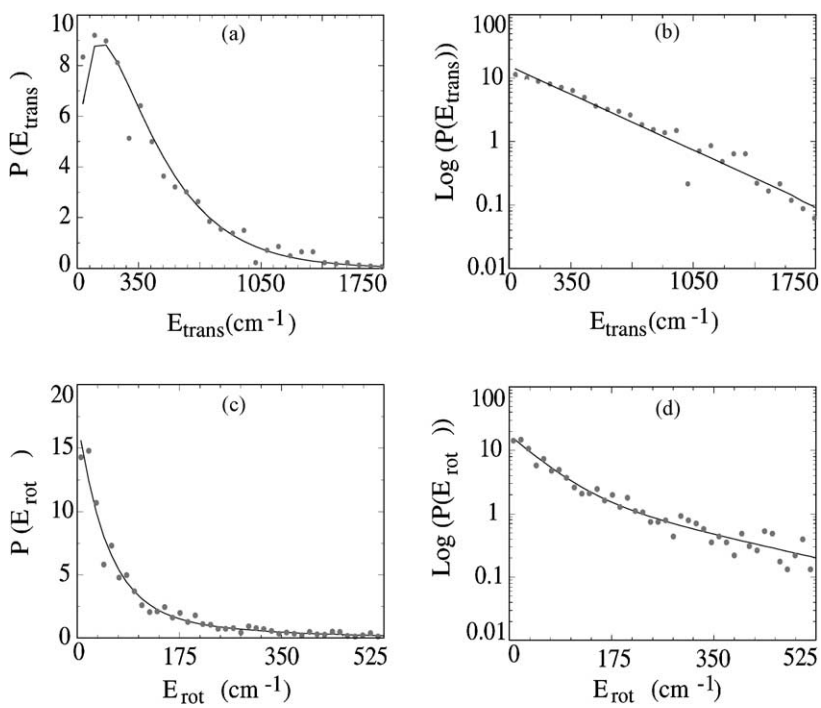

Fig. 6. Translational and rotational distributions obtained at $\theta_i = 30°$ and a cluster of 512 molecules. Upper plots: one translational temperature distribution. Lower plots: two rotational temperature distribution. Circles represent the simulated values and solid lines are Boltzmann fits to the simulated data.

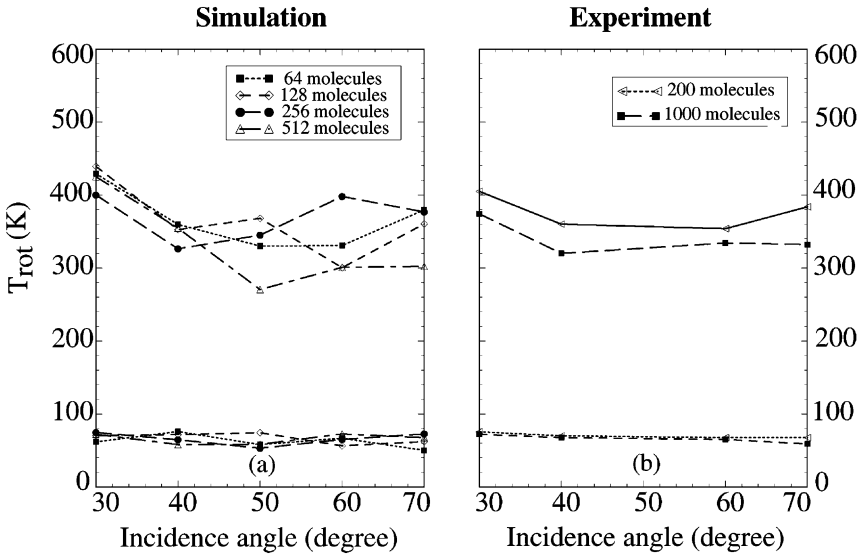

Fig. 7. Evolution of the rotational temperature with incident angle and cluster size.

We actually performed the same simulations for an incident cluster velocity of 1440 m s^{-1} and we found roughly the same rotational temperatures of 75 and 375 K. While the rotational temperatures remain almost unchanged in spite of a nearly four times larger incident kinetic energy, the relative importance of the cold component decreases by a factor of two and the translational temperature nearly scales with the increase in incident kinetic energy. This is clearly due to shattering that becomes strongly enhanced by the much more violent impact. The fact that the rotational energy does not increase while the translational one does suggests a process with very efficient rotational hindrance [34]. In fact, Gadzuk et al. [34] previously proposed such a process to explain why the rotational temperature of individual molecules scattering from solid surfaces first increases linearly with surface temperature, but then saturates at a constant value of about 250 to 350 K even for surface temperatures as high as 900 K.

To better understand the physical origin of the two distinct rotational distributions, we show in Fig. 8(a) that molecules from the two different rotational components originate from cluster areas that can be characterized by clearly different densities. In fact, the existence of two densities, even before the impact event, clearly demonstrates that the component corresponding to higher densities originates from the initial center of the cluster, whereas the lower-density molecules evaporate from the outskirts of the cluster. More specifically, we define cold molecules as monomers with rotational energy less than 0.3 kcal mol^{-1} (i.e., a rotational quantum number smaller than $J = 7$) and hot molecules as having rotational energy larger than 0.6 kcal mol^{-1} (i.e., a rotational quantum number that is larger than $J = 11$). The cluster compression taking place during the first 0.8 ps after impact causes a density increase for both components. Both densities start decreasing as soon as monomer evaporation becomes significant. The averaged densities change with incidence angle; for large incidence angles the density distributions becomes more flat (see Fig. 8(c)). The density difference between the two rotational components is more pronounced for the larger incidence angles. This is consistent with the fact that, at 40° impact, the two cluster zones are more compressed than at 60°, and the number of molecules contributing to the hot component is considerably larger than at 60°. Therefore, only the outermost cluster molecules contribute to the

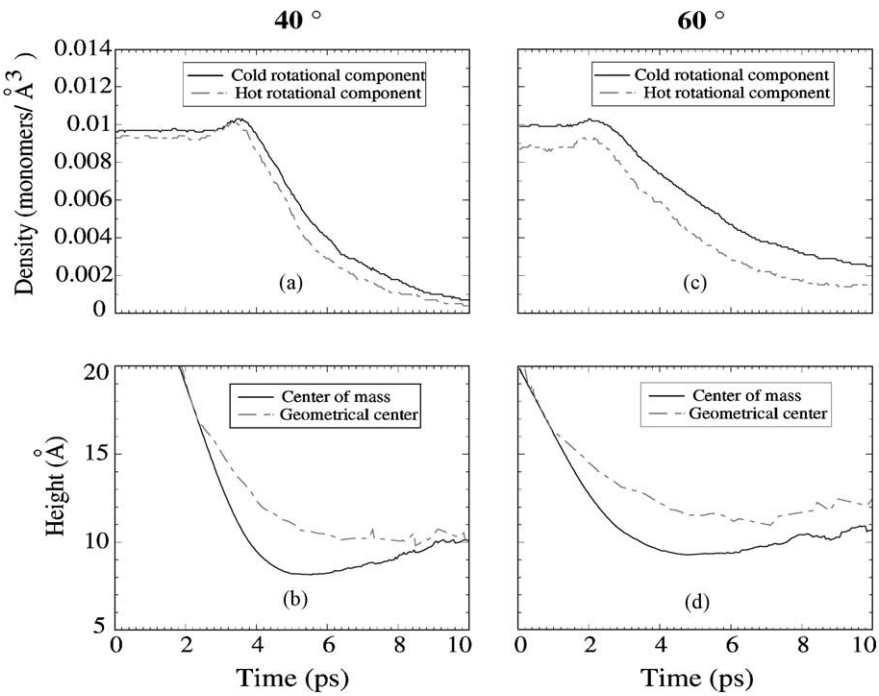

Fig. 8. Comparison between simulated density distributions around each monomer in a surviving cluster gliding on the surface as a function of time (in ps), for incidence angles 40° (a) and 60° (c), an incident cluster size of 512 molecules and a surface temperature of 580 K; (b) and (d) show the time evolution of the height of the center of mass and of the geometrical center of the cluster for the same conditions as above. Time zero denotes again the beginning of our trajectory calculations.

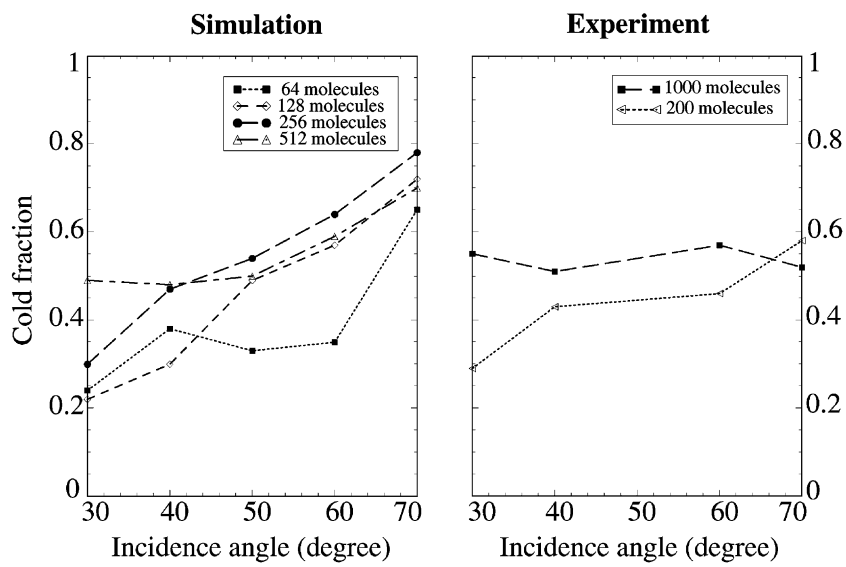

Fig. 9. Simulated and experimental results for the importance of the cold component as function of incidence angle and cluster size with a 580 K graphite surface.

hot component for a 60° incidence angle, resulting in a larger average density difference than for 40°.

We like to point out that the density around rotationally hot monomers at an incidence angle of 60° is lower than around those at 40° even before the impact event, since the assignment of the evaporated molecules in "hot" and "cold" rotational components can only be accomplished at the end of the scattering process and since the density of a thermalized cluster is somewhat higher in the center of the cluster than in the outermost layers. At large incidence angles, for example, hot monomers only originate from the very outskirts of the cluster, while at 40°, the hot component is composed of molecules that were localized in a thicker external layer of the cluster. When the incidence angle approaches very low values, there is no more marked vapor cushion and the distinction between the two zones of the cluster becomes less obvious, as shown in Fig. 8(a), where the densities around rotationally hot and cold monomers are, indeed, very similar before the impact. For the longest simulation times shown, the absolute densities for the smaller incidence angle are lower than for the larger one. Tentatively, we attribute this observation to the difference in cluster temperature at 10 ps (see Fig. 5(a)).

Let us now consider the detailed zone structure of the cluster during the scattering event. Besides the dominant evaporation components described above, we would also like to demonstrate the existence of another region in the cluster. In Fig. 8(b) and (d), we represent the evolution of the height of the center of mass and of the geometrical center of the surviving cluster measured from the graphite surface. For both incidence angles, the center of mass approaches closer to the surface than the geometrical center of the cluster indicating the formation of a relatively dense "vapor cushion" throughout the scattering process. When the surviving cluster leaves the surface, the two centers become nearly identical as they were before the surface impact. For a 60° incidence angle, the cluster

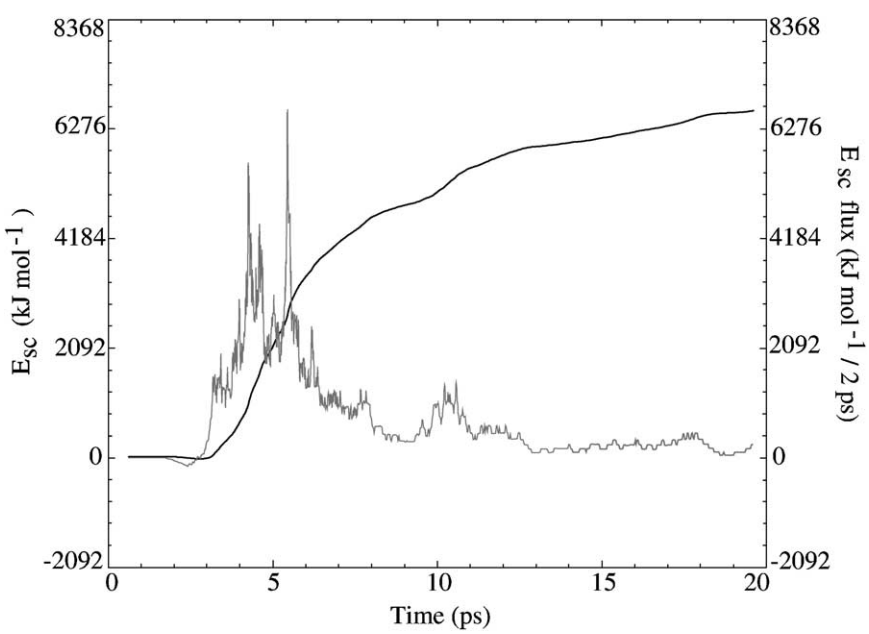

Fig. 10. Integrated energy E_{sc} transferred from the surface to a nitrogen cluster of 512 molecules for an incidence angle of $\theta_i = 40°$ and a surface temperature of 580 K as a function of time (thick smooth curve, left scale). The thin curve is obtained from time differentiation of the first curve and represents the time evolution of the energy flux from the surface to the cluster (right scale). The time "$t = 0$" corresponds again to the beginning of the trajectory calculations.

glides on the surface for a longer period of time than at 40°, since the normal component of the incident energy is less, resulting in milder impact conditions. In summary, we propose that the rotationally hot component of monomer evaporation takes place from the outer layers of the cluster, where they are more free to move than in the dense zone in the very cluster center that gets in contact with the surface during the time the cluster glides along the surface. Consequently, the higher-density zone from which the cold component originates can directly be related to the vapor cushion. Because of steric constraints, the monomers of the cold component are well caged during cluster impact and shortly after, and they can only evaporate at much later times than do the hot component molecules. The cold fraction W_{cold} is shown in Fig. 9 where it can be seen that the importance of this cold component increases with incidence angle θ_i. The same trend can be observed in the experimental results for $(N_2)_{200}$, and can be attributed to the fact that there are relatively more molecules that evaporate during the very early stages of the scattering process for smaller incidence angles, i.e., the smaller the incidence angle, the more important the hot component becomes. Moreover, W_{cold} slightly increases with cluster size because the proportion of molecules in the very interior relative to that at the outskirts of the cluster increases with cluster size.

In Fig. 10, we finally show the evolution of the integrated energy E_{sc} transferred from the surface to the cluster, and the corresponding energy flux as a function of time. At impact, the energy flux becomes slightly negative because the surface absorbs some of the incident normal translational energy of the incoming cluster due to surface trapping. When trapped monomers start desorbing from the surface again, the energy E_{sc} becomes largely positive and increases until about 15 ps, when it stabilizes since all surface-trapped molecules have desorbed by then.

4. Conclusion

In the present study, molecular dynamics simulations employing a simple trapping/desorption scheme to model a solid surface has enabled us to reproduce the parallel velocity conservation factor c_F, the translational temperature and rotational temperatures of evaporated monomers obtained experimentally. Our model does not only give a qualitative image of the evaporation of monomers resulting from the impact of large clusters onto a graphite surface, but it also gives correct quantitative results without the use of any fitting parameters. In fact, instead of using the nitrogen molecule–surface binding energy E_s as a fitting parameter, we use the E_s value that has been experimentally determined by Vidali et al. [29].

Analysis of the dynamics of the cluster scattering event in terms of the DZS model supports the energy transfer mechanisms proposed in an earlier theoretical study [19]. The trends in the c_F with incidence angle and surface temperature suggest that a large portion of the monomers that form the cluster do not interact directly with the surface. This implies that an isolating vapor cushion is formed from monomers that are trapped between the surface and other incoming monomers, as suggested in the DZS model. Analysis of the translational temperature changes with incidence angle and cluster size, and the time evolution of the instantaneous cluster temperature, indicate that degree of translational excitation of the product monomers depends on the instantaneous cluster temperature at which the monomers evaporate. The time evolution of the density around rotationally hot and cold monomers demonstrates the existence of two zones, besides the vapor cushion, from which monomers evaporate: the outskirts of the cluster and the surviving cluster which is comprised of monomers that were trapped within the cluster during impact. The trends in the two rotational temperatures strongly suggest that the rotationally hot monomers are subject to rotational hindrance upon evaporation from the surface of the moving cluster, whereas rotationally cold monomers evaporate from the surviving cluster at a temperature which depends on the stabilized instantaneous cluster temperature.

In conclusion, the dynamics of the cluster scattering event reported here, as well as the redistribution

of the impact energy into translational and rotational degrees of freedom, paints a picture in very good agreement with the basic features of the DZS model [16].

Acknowledgements

Most of the calculations were carried out at the French National Computer Center IDRIS and at the Centre for Research in Molecular Modeling (CERMM, Montréal, Québec, Canada), which was established with the financial support of the Concordia University Faculty of Arts & Science, the Ministére de l'Éducation du Québec (MEQ) and the Canada Foundation for Innovation (CFI). We like to acknowledge the computer time that was allotted for the present study at IDRIS. We also thank those at the Laboratory PICM and the computer center of the Ecole Polytechnique DSI who helped us to complete this current work. This work was funded in part by a research grant from the Natural Science and Engineering Research Council (NSERC) of Canada. D.M.K. is a recipient of NSERC and Concordia University graduate fellowships.

References

[1] T. Raz, R.D. Levine, Chem. Phys. Lett. 246 (1995) 405.
[2] J.D. Beckerle, A.D. Johnson, S.T. Ceyer, J. Chem. Phys. 93 (1990) 4047.
[3] J. Gspann, G. Krieg, J. Chem. Phys. 61 (1974) 4037.
[4] R.J. Holland, G.Q. Xu, J. Levkoff, J. Robertson, S.L. Bernasek, J. Chem. Phys. 88 (1988) 7952.
[5] A. Vostrikov, D. Dubov, Z. Phys. D 20 (1991) 61.
[6] M. Châtelet, A. De Martino, J.B.C. Petterson, F. Pradère, H. Vach, Chem. Phys. Lett. 196 (1992) 563.
[7] H. Vach, A. De Martino, M. Benslimane, M. Châtelet, F. Pradère, J. Chem. Phys. 100 (1994) 3526.
[8] M. Benslimane, M. Châtelet, A.D. Martino, F. Pradère, H. Vach, Chem. Phys. Lett. 237 (1995) 323.
[9] A. De Martino, M. Benslimane, M. Châtelet, F. Pradère, H. Vach, J. Chem. Phys. 105 (1996) 7828.
[10] C. Menzel, A. Knoner, J. Kurtzner, H. Zacharias, Z. Phys. D 38 (1996) 179.
[11] F. Pradère, M. Benslimane, M. Châtelet, A. De Martino, H. Vach, Surf. Sci. Lett. 375 (1997) L375.
[12] G.Q. Xu, S.L. Bernasek, J.C. Tully, J. Chem. Phys. 88 (1988) 3376.
[13] G.Q. Xu, S.L.B.R.J. Holland, J.C. Tully, J. Chem. Phys. 90 (1989) 3831.
[14] J.B.C. Pettersson, N. Markovic, Chem. Phys. Lett. 201 (1993) 421.
[15] N. Markovic, J.B.C. Pettersson, J. Chem. Phys. 100 (1994) 3911.
[16] H. Vach, M. Benslimane, M. Châtelet, A. De Martino, F. Pradère, J. Chem. Phys. 103 (1995) 1972.
[17] M. Svanberg, N. Markovic, J.B.C. Pettersson, Chem. Phys. 201 (1995) 473.
[18] A. De Martino, M. Châtelet, F. Pradère, H. Vach, J. Chem. Phys. 111 (1999) 7038.
[19] D.M. Koch, G.H. Peslherbe, H. Vach, J. Chem. Phys. 115 (2001) 7685.
[20] H. Kono, S.H. Lin, J. Chem. Phys. 78 (1983) 2607.
[21] M.D. Alvey, J.T. Yates, K.J. Uram, J. Chem. Phys. 87 (1987) 7221.
[22] M.P. Allen, D.J. Tildesley, Computer Simulation of Liquids, Clarendon Press, Oxford, 1994.
[23] W.H. Press, W.T. Vetterling, S.A. Teukolsky, B.P. Flannery, Numerical Recepies in Fortran 77, Cambridge University Press, Cambridge, 1999.
[24] R. Viswanathan, D.L. Thompson, L.M. Raff, J. Chem. Phys. 80 (1984) 4230.
[25] J.I. Steinfeld, J.S. Francisco, W.L. Hase, Chemical Kinetics and Dynamics, 1998.
[26] J. Farges, B. de Feraudy, B. Raoult, G. Torchet, J. Chem. Phys. 44 (1986) 3491.
[27] H. Vach, Phys. Rev. B 61 (2000) 2310.
[28] M. Head-Gordon, J.C. Tully, J. Chem. Phys. 94 (1990) 1516.
[29] G. Vidali, G. Ihm, H.Y. Kim, M.W. Cole, Surf. Sci. Rep. 12 (1991) 133.
[30] J. Frenkel, Z. Phys. 26 (1924) 117.
[31] M.C. Gutzwiller, Chaos in Classical and Quantum Mechanics, Springer, New York, 1990.
[32] H. Vach, A.D. Martino, M. Benslimane, M. Châtelet, F. Pradère, J. Chem. Phys. 100 (1994) 8526.
[33] P.U. Andersson, A. Tomsic, M.B. Andersson, J.B.C. Pettersson, Chem. Phys. Lett. 279 (1997) 100.
[34] J.W. Gadzuk, U. Landman, E.J. Kuster, C.L. Cleveland, R.N. Barnett, Phys. Rev. Lett. 49 (1982) 426.